PERGAMON

Journal of Structural Geology 22 (2000) 1837–1853

JOURNAL OF STRUCTURAL GEOLOGY

www.elsevier.nl/locate/jstrugeo

The Chinamora batholith, Zimbabwe: structure and emplacement-related magnetic rock fabric

J.K. Becker[a,*], S. Siegesmund[a], H.A. Jelsma[b]

[a]*Institut für Geologie und Dynamik der Lithosphäre, Universität Göttingen, Goldschmidtstr. 3, 37077 Göttingen, Germany*
[b]*University of Zimbabwe, Department of Geology, P.O. Box MP167, Harare, Zimbabwe*

Received 29 November 1999; accepted 9 May 2000

Abstract

The origin of dome-and-keel structural geometries in Archean granite–greenstone terrains appears to lack any modern analogues and is still poorly understood. The formation of these geometries is investigated using structural and anisotropy of magnetic susceptibility (AMS) data for the Chinamora batholith in Zimbabwe. The roughly circular-shaped batholith is surrounded by ca. 2.72–2.64 Ga greenstones. The batholith granitoid suites have been divided on the basis of their ages and fabric relationships into four distinct units: (i) banded basement gneisses; (ii) granodioritic gneisses; (iii) equigranular granites; and (iv) central porphyritic granites. In the gneissic granites a partial girdle (N–S) of poles to the magnetic foliation is developed that has been folded around a consistent, flat lying magnetic lineation plunging at shallow angles to the E or W. In the equigranular granites, the magnetic lineation generally plunges to the NW. The magnetic foliation has a variable strike, no clear trends can be distinguished. The AMS measurements of the porphyritic granite revealed a NW–SE striking foliation and showed subhorizontal magnetic lineations. The magnetic foliation is subparallel to the macroscopic foliation. Wall rocks are moderately inclined and show radial or concentric lineations, triaxial strain ellipsoids and kinematics that demonstrate off-the-dome sliding and coeval pluton expansion. The results of the observations do not point to a single emplacement process. Neither the observed structural data nor the magnetic fabric support a model envisaging spherically 'ballooning'. It is argued that pluton diapirism played a major part in the formation of the fabrics in the gneisses, whereas the fabrics in the porphyritic granites reflect emplacement as laccolith-like sheets.

1. Introduction

In the Pilbara and parts of the Dharwar and Zimbabwe cratons, granite–greenstone terrains are characterized by dome-and-keel geometries that appear to lack any modern analogues. Such structural patterns have been proposed to be the result of a number of processes such as: (i) solid-state or magmatic diapirism (Macgregor, 1951; Hickman, 1984; Collins, 1989; Jelsma et al., 1993; Bouhallier et al., 1993, 1995), or partial convective overturn of the crust (Collins et al., 1998); (ii) ballooning through inflation of plutons (Ramsay, 1989); (iii) cross folding (Snowden and Bickle, 1976; Bickle et al., 1980; Myers and Watkins, 1985), non-cylindrical folding (Platt, 1980; Schwerdtner, 1990); and (iv) the formation of magmatically induced, Cordilleran-style metamorphic core complexes (Zeegers et al., 1996), or a combination of these processes.

Gravity has long been proposed as a driving mechanism in the formation of dome-and-keel structural patterns (Eskola, 1947; Macgregor, 1951). Laboratory experiments (Dixon, 1975; Schwerdtner and Troeng, 1978; Dixon and Summers, 1983; Cruden, 1988) and computer analogue models (Mareschal and West, 1980; Van Berkel, 1988; Schmeling et al., 1988; Weinberg and Schmeling, 1992) have shown that gravity and diapirism are theoretically valid driving and ascent/emplacement mechanisms under certain conditions and up to certain depths (Weinberg and Podladchikov, 1994). Structural and metamorphic criteria that can be used to recognize pluton diapirs include: (i) strain intensification towards the contacts with surrounding wall rocks, with a penetrative, concentric foliation or schistosity within marginal zones; (ii) formation of cleavage triple points (CTPs) in between three or more domes or near a contact that trends at a high angle to the regional foliation; (iii) radial or tangential patterns of stretching lineations; (iv) a strain state in marginal zones ranging from radial oblate to triaxial flattening strain; (v) kinematics of contact shear zones giving a dome-side-up sense of movement; and (vi) thermal aureoles and pre- to syn-kinematic porphyroblast growth (in case of thermal relaxation) in the adjacent wall

* Corresponding author.

0191-8141/00/$ - see front matter
PII: S0191-8141(00)00061-4

rocks (Bateman 1984; Van den Eeckhout et al., 1986; Paterson and Tobisch 1988; Jelsma et al., 1993; Ridley et al., 1997; Clemens et al., 1997). In addition, the pluton diapirs are circular or ovoid in shape and comprise rocks with a lower density than the average density of the cover rocks.

Many of the above features of diapiric structures are identical to those we would expect for ballooning structures (England, 1990) or non-cylindrical folds (Veenhof and Stel, 1991). Ballooning does not include the actual ascent mechanism but describes the inflation of a granitoid body at the point where magma is in a state of neutral buoyancy, or is trapped by structure, rheological heterogeneities and/or by a balance between magma pressure and lithostatic load (Clemens and Mawer, 1992; Vigneresse, 1995; Hogan and Gilbert, 1995; Hogan et al., 1998). Ballooning may include the inflation of a pluton or laccolith. The enveloping rocks should show signs of pure flattening strain with finite strain ellipsoids paralleling the outer margin of the body. Diapirism and ballooning are thus two end-members of emplacement mechanisms with a fluent transition in between and may not be mutually exclusive (Brun and Pons, 1981). In the case of ballooning itself, a concentric margin parallel foliation should develop with decreasing distinctness towards the center of the pluton (see Siegesmund and Becker, in press). A radial lineation may be developed near the center of the intrusion pointing towards the contact area which displays the direction of inflation and tangential lineations can be expected along the actual contact.

Non-cylindrical folds may have similar surface shapes to diapiric or ballooning structures and, as for these structures, may show high strain gradients near marginal zones. This is particularly so if the batholiths were rigid, pre-tectonic structures, but also holds for syn-tectonic structures. The dome-side-up shear sense of diapiric structures contradicts the shear sense associated with flexural-slip folds but conforms that of buckle folds. Non-cylindrical folds, however, cannot explain the presence of cleavage triple points. They are furthermore characterized by lineation trajectories that converge towards a straight trend across the midlines of domes (Schwerdtner, 1990; Veenhof and Stel, 1991), which is at variance to the lineation trajectories of diapiric or ballooning structures.

Core complexes also have a similar appearance to many of the above structures (cf. Lister and Davis, 1989). Zeegers et al. (1996), for example, describe structures and kinematic relations in the Pilbara craton that are consistent with doming during greenstone deposition in an extensional tectonic environment. Core complexes are characterized by parallellism of foliations in the batholiths and greenstones, a ductile detachment zone at the contact, unidirectional stretching lineations, and a consistent transport direction across the domal geometry.

The Chinamora batholith is a good example for the discussion of emplacement mechanisms. The Chinamora batholith occurs in the northern part of the Zimbabwe craton (see Fig. 1a). As in the Pilbara craton, this part of the craton is characterized by a large number of ellipsoidal plutons or batholiths, which are surrounded by greenstone belts (see Fig. 1b). Numerous authors have contributed their data to the emplacement model of the Chinamora batholith, yet no generally accepted model exists. Only the late granites (porphyritic granites) have generally been interpreted as tabular sheets (Snowden, 1976; Baldock, 1990; Jelsma, 1993), that may have been fed by dyke-like conduits (Treloar, 1997).

To test different emplacement models, an intensive study of the magnetic properties of the different rock suites of the classical Chinamora batholith has been performed, including anisotropy of magnetic susceptibility (AMS) measurements. Since some samples showed very high bulk susceptibilities, high field analyses on some selected samples have been performed to separate the AMS of the paramagnetic and ferrimagnetic minerals. Thin sections have been prepared to test the significance of the AMS and high field analyses (HFA) data with the macroscopic and microscopic rock fabric. The qualitative ore mineralogy was obtained from measurements with the Curie-balance.

2. Regional geology

2.1. Field relations and petrography of rock units within the Chinamora batholith

The Chinamora batholith comprises at least 26 different lithologies (Snowden, 1976; Snowden and Bickle, 1976; Snowden and Snowden, 1979, 1981) which on the basis of their fabric and their age relationship can be grouped into four major units: (i) banded gneiss (possible basement); (ii) gneissic granites; (iii) equigranular granites; and (iv) porphyritic granites in the center of the batholith (where i is the oldest and iv the youngest unit). The outcrop area of the basement gneiss in the Chinamora batholith is widely scattered and can be observed in erosional windows in the porphyritic granite as well as in marginal areas in the gneissic granites near the Umwindsi shear zone (see Fig. 1b). They consist of tightly folded, banded, xenolith-bearing migmatites that have been reworked during later tectonothermal events, probably the intrusions of the younger granitic suites. The simplest classification of the basement gneiss is into biotite gneiss (melanosomes) and quartzofeldspathic gneiss (leucosomes), yet their appearance differs widely between the different outcrops. Only in the area east of the Umwindsi shear zone, is the banded nature of the gneisses obvious. Erosional windows in the porphyritic granite rocks, which have been referred to as basement gneiss (Snowden, 1976), are similar to the marginal gneissic granites, and these occurrences have therefore been assigned by us to the gneissic granites.

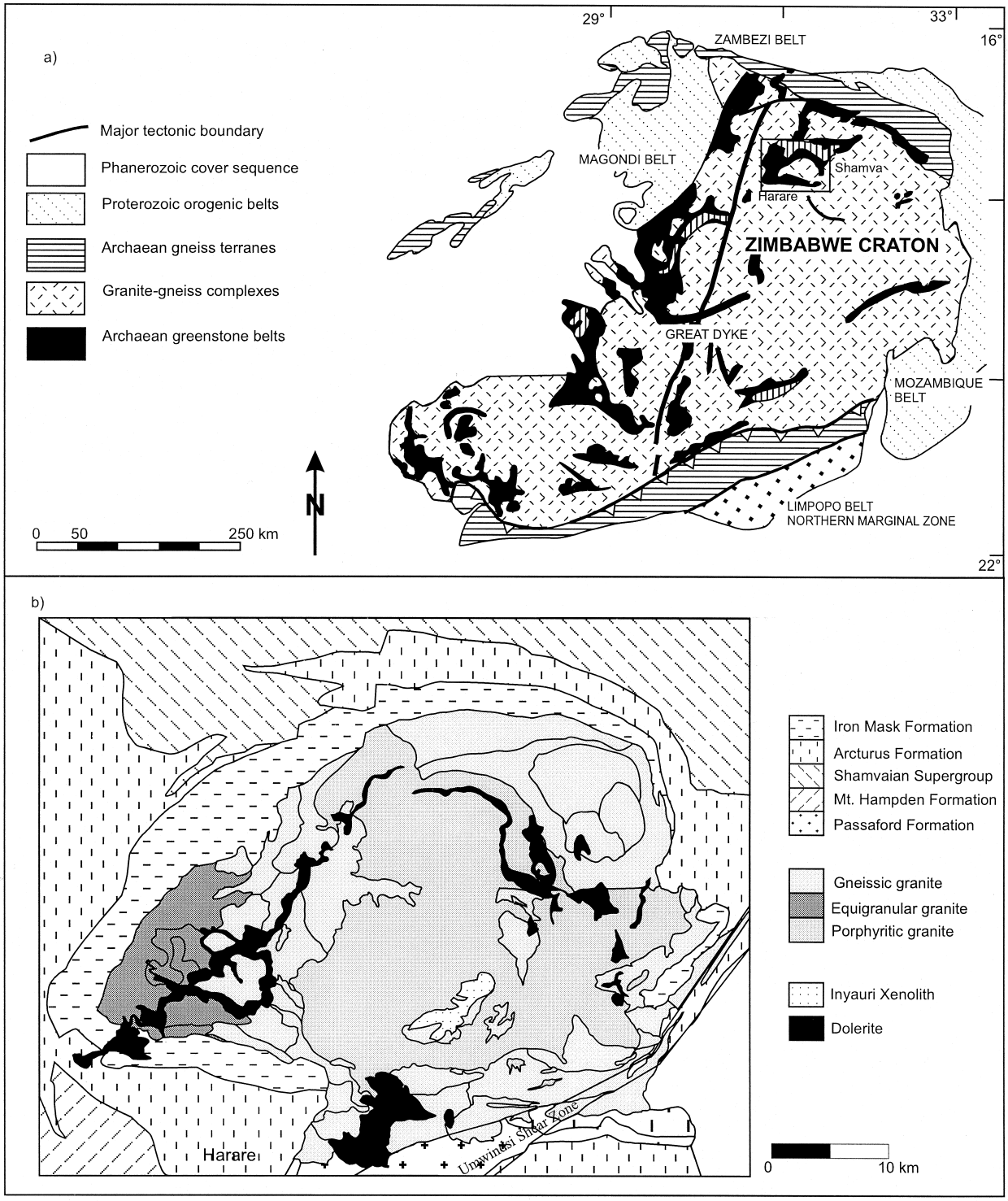

Fig. 1. (a) Overview of the Zimbabwe craton. The Chinamora batholith is boxed. (b) Lithologies and surrounding greenstone belts in the area of the Chinamora batholith (solid lines represent lithological boundaries).

The gneissic granites envelope the porphyritic granites and form the outer margin of the batholith, except for the western areas where they are bound by the equigranular granites. They have a relatively high mafic mineral content (up to 40%), are usually strongly foliated and show dark, hornblende-bearing xenoliths that have lengths up to 2 m. On the Streckeisen diagram (Fig. 2) the gneissic granites show a wide variety of modal compositions ranging from quartz-rich tonalite (trondhjemite) to a quartz depleted monzogranite/syenogranite. Between these two

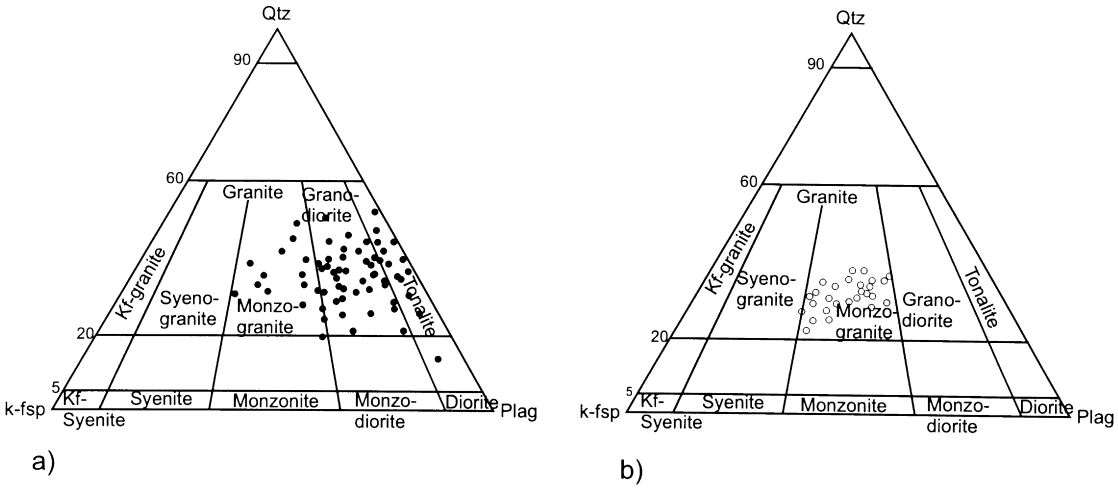

Fig. 2. Streckeisen diagram of the gneissic granites (a) and the porphyritic granite (b). See text for details.

end-members a range of modal compositions can be found. According to their macroscopic fabric and geographical distribution the gneisses have been divided into three units: the northeastern (Fig. 3C), northwestern (Fig. 3D) and southern gneisses (Fig. 3A and B). The marginal gneissic granites show features indicative of solid-state deformation, but microstructures show that the southern gneisses suffered more intense deformation than the northern ones (compare Fig. 3A and C). In the southern gneisses, elongate quartz grains with chessboard subgrain patterns, bending of plagioclase twin lamellae, as well as the presence of anhedral garnet porphyroblasts are common

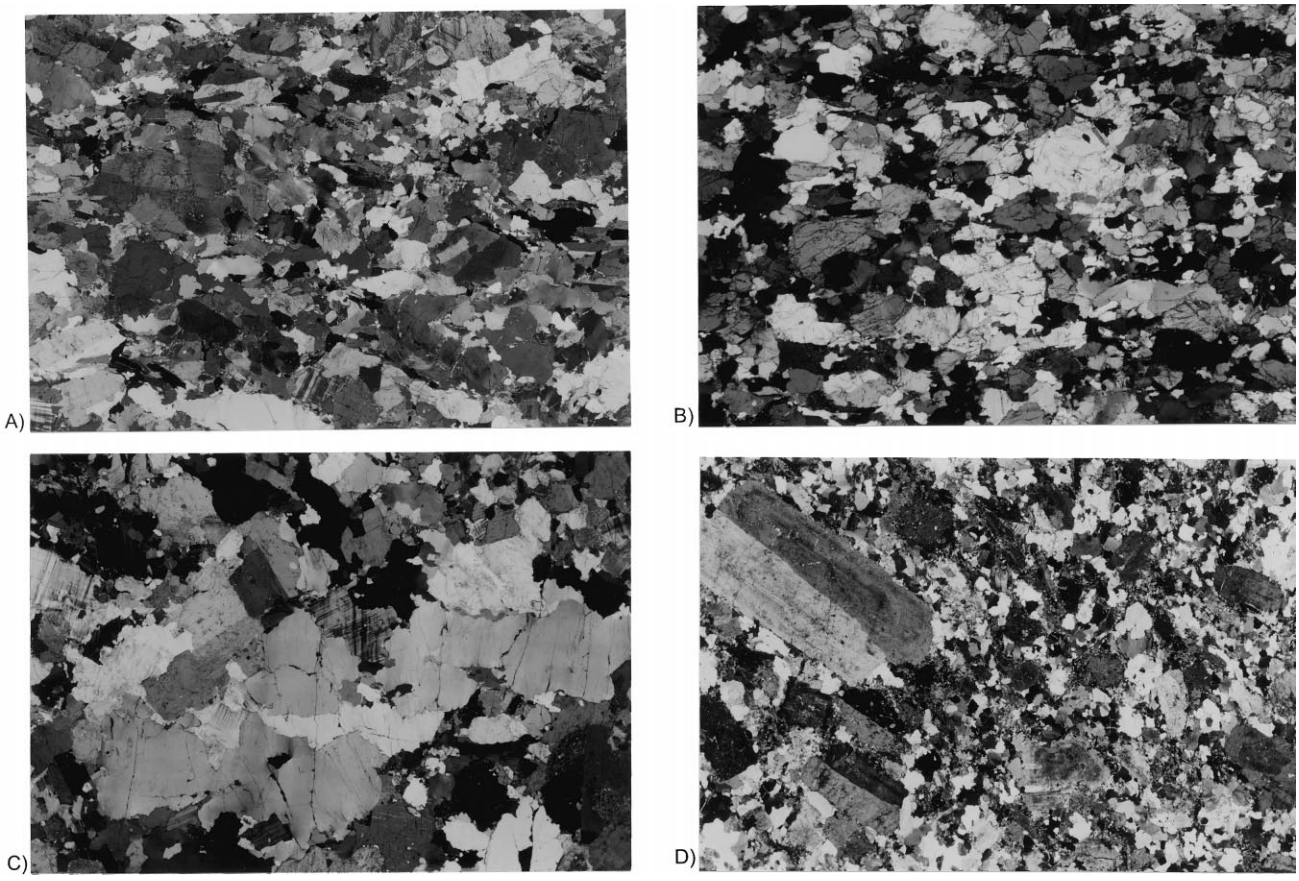

Fig. 3. (A) SC-fabric in the southern gneissic granites mainly defined by hornblendes and feldspars. (B) SC-fabric in the southern gneissic granites defined by biotites, feldspars and quartz. Note that some biotites show mica-fishes. (C) Elongate quartz grains in the northeastern gneissic granites indicating a solid-state overprint of the magmatic fabric. (D) Large feldspars and hornblendes in a matrix of recrystallized quartz grains in the northwestern gneissic granites.

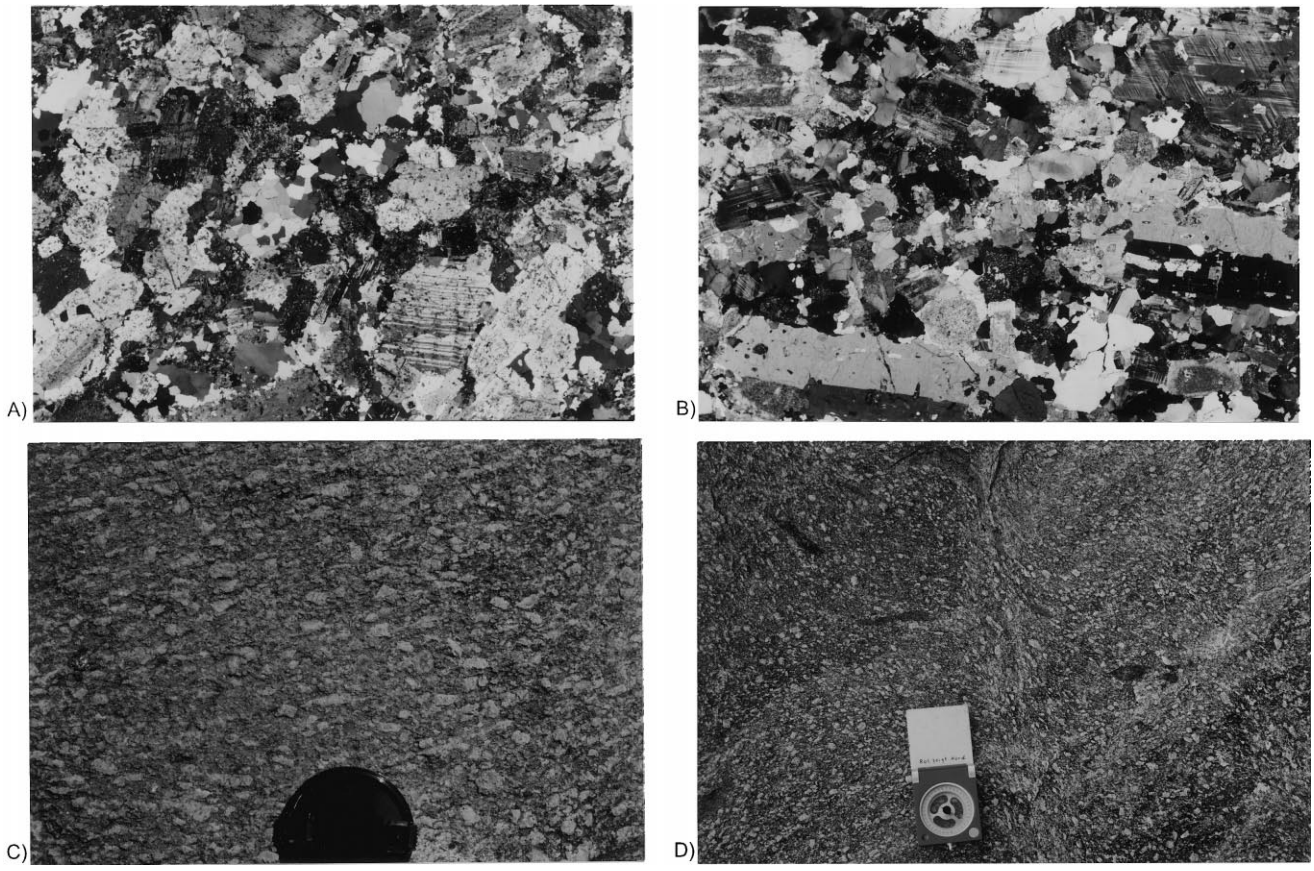

Fig. 4. (A) Microphotograph of the equigranular granites. Feldspars are strongly altered and show signs of a weak solid-state overprint (deformation lamellas, bend twin lamellas in feldspars). (B) The porphyritic granite shows aligned megacrysts of plagioclase and k-feldspars that incorporated other minerals during growth. The inclusions reflect the same mineralogy as the host rock. (C) Megacryst alignment in the porphyritic granite. Tiling of megacrysts is scarce. (D) Small-scale shear zone indicating dextral sense of shear. The photograph was taken in the contact area of the porphyritic granites to the gneissic granites.

observations. In the northern gneisses, quartz grains show the typical chessboard subgrain pattern and irregular grain boundaries that can also be found in the southern gneisses, but elongate quartz grains are rare. Truly solid-state shear zones only occur in the southern gneisses with small, dynamically recrystallized quartz grains and offset of grains. The macroscopic foliation in the gneisses is in all localities parallel to the batholith margin. The angle of dip is moderate, ranging between 40 and 60° (see Fig. 5b).

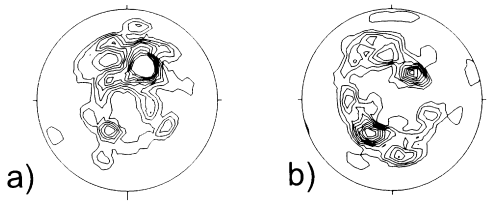

Fig. 5. Macroscopic foliation of the gneissic granites (a) and the porphyritic granite (b) (lower hemisphere, density plots are computed using equal-area algorithms, applies to all presented pole figures). While the porphyritic granite shows a preferred dip to the south foliations of the gneissic granites nearly define a small circle indicating their margin parallel strike. The two strong point maxima can be explained in terms of sample density in the north and south of the batholith.

Small scale shear zones are abundant in the gneissic granites (Fig. 4D).

The area in between the Chinamora and Murehwa batholiths has been referred to as the Umwindsi shear zone (Jelsma, 1993; Huizenga, 1995). The shear zone has a width of approximately 200 m and a length of at least 15 km. The main structure occurs in hornblende schists and shows a well-developed foliation and mineral lineation. The foliation dips at a steep angle of 70–90° to the northwest. The lineation is defined by hornblende and plunges at 35° to the southwest. The shear zone shows a sinistral sense of movement and an upward movement of the southeastern block. Near the Umwindsi shear zone, the gneissic granites show weak S–C fabrics (Fig. 3A) accommodating a sinistral sense of shear, with hornblende crystals defining the *S*-plane. The shear deformation is thought to be contemporaneous with the M_2 peak metamorphism in the adjacent greenstone belt (see below), that is upper amphibolite to granulite facies conditions of metamorphism.

Amongst the late granites, the equigranular granites (Fig. 4A) contain less than 5% of mafic minerals. Their modal composition ranges from tonalite/trondhjemite to monzogranite but concentrates in the field of quartz-rich

granodiorite. The porphyritic granite in the center of the batholith has an areal extent of approximately 600 km^2 and is commonly bordered by the gneissic granites. Exceptions to this occur in the western areas where the equigranular granites impinge against the porphyritic granite or where the porphyritic granite is in direct contact with the greenstone belt. A prominent characteristic of the porphyritic granite is the alignment of feldspar megacrysts which range in size between 2 and 5 cm in length (see Fig. 4B and C). The modal composition of this rock suite is mainly monzogranitic with a low to moderate quartz content. Some syenogranitic rocks do occur (Fig. 2b). The porphyritic granite only shows magmatic to submagmatic fabrics. The most common features in the porphyritic granite are myrmekitic intergrowth, microcracks in feldspars healed with quartz or feldspars and the typical chessboard subgrain patterns in quartz. Some of the plagioclases have slightly bent twin lamellas indicating a transition between magmatic and high-temperature solid-state origin. The feldspar phenocrysts are of truly magmatic origin since during growth they incorporated other minerals like feldspars and biotites along crystal faces. Biotites in the porphyritic granite seem to wrap around the feldspar phenocrysts building only loosely interconnected weak layers. Foliation planes in the porphyritic granite trend NW–SE with a preferred dip to the SW. Only in some areas near the contact with other lithologies is this strike margin parallel. The angle of dip is usually moderate, ranging between 30 and 50° (see Fig. 4B). Only at the northern margin of the porphyritic granite the foliation dips to the NE.

The Inyauri xenolith (Fig. 2) occurs in the southcentral part of the Chinamora batholith. The unit has an outcrop area of 8×2 km comprising hornblende-biotite schists and is often described as a xenolith (roof pendant) in the porphyritic granite. According to the topographical and geological maps the xenolith surface is approximately 60 m lower than the surrounding surface of the gneissic granites so it may as well be a xenolith contained by underlying gneissic granites.

2.2. Age data for the Chinamora rock suites

The age data on the granitoids are limited. Banded gneisses along the western margin of the Murehwa batholith, adjacent to the Chinamora batholith, have been dated by Baldock and Evans (1988) at 2865 ± 135 Ma (Rb–Sr whole-rock), suggesting that these form basement to the greenstone sequence. Gneissic granitoids near the eastern margin of the Chinamora batholith have been dated by the same authors at 2680 ± 102 Ma (Rb–Sr whole-rock) and by Jelsma et al. (1996) at 2667 ± 4 Ma (U–Pb TIMS zircon). Syn- to post-tectonic granodiorites and tonalites, intrusive into the greenstone belt and equated with the equigranular late granites within the Chinamora batholith, have yielded U–Pb TIMS zircon ages of 2664 ± 15 Ma (Mazowe), 2649 ± 6 Ma (Bindura) and 2618 ± 6 Ma (Glendale) (Jelsma et al., 1996). However, felsic volcanics that host the Mazowe granodiorite (and are hence supposed to be older in age) have been dated at 2643 ± 8 Ma (Wilson et al., 1995). This may indicate that some of the TIMS zircon ages reflect mixing between magmatic and inherited basement components. A U–Pb TIMS zircon age of 2601 ± 14 Ma constrains the age of supposedly post-tectonic porphyritic granites in the Murehwa batholith to the east. These granites may form part of the ca. 2.6 Ga Chilimanzi intrusive event that affected large parts of the craton (Wilson et al., 1995; Jelsma et al., 1996).

2.3. Greenstone wall rocks

The Chinamora batholith has been wrapped around by metavolcanics and metasediments of the Harare-Shamva greenstone belt. These greenstones have been assigned to the upper Bulawayan Supergroup (mostly bimodal volcanics) and the overlying Shamvaian Supergroup (mostly sediments). The age of the volcanics is bracketed between 2715 and 2643 Ma (Wilson et al., 1995; Jelsma et al., 1996; see Fig. 1). The stratigraphy and structure of the greenstone belt have been described in detail by Jelsma et al. (1993) and Jelsma and Dirks (2000).

The Harare-Shamva greenstone belt defines a complex, arcuate and apparently synclinal structure with the core of the syncline consisting of Shamvaian sediments and the flanks of Bulawayan volcanics (Fig. 1). The basal succession of the greenstone belt is represented by a 3–9 km thick bimodal suite of rhyodacites and basalts. Intercalated are horizons of ultramafic rocks, graphitic argillites, iron stones, marble, chert and conglomerate. This succession is unconformably overlain by clastic sediments that reach a thickness of approximately 1–2 km (Jelsma, 1993). Intrusive into the Upper Bulawayan and Shamvaian lithologies are various small plutonic bodies that have been dated between ca. 2.66 and 2.62 Ga (Jelsma et al., 1996).

2.4. Deformational events

Snowden and Bickle (1976) recognized three different deformation events (D_1–D_3), with the second and third events resulting in large-scale interference folding. They concluded that the D_2 event was caused by NW–SE compression, and that during D_3 the rigid and brittle crust was buckled, giving rise to the dome-and-keel granite–greenstone terrain. They proposed that the feldspar megacryst alignment in the porphyritic granites was formed during the D_2 event and was folded during the D_3 event.

Ramsay (1989) divided the rock suites into central adamellite (comparable to the porphyritic granite), western adamellitic granite (includes the late granites and part of the gneissic granites), tonalite (includes the old gneisses and part of the gneissic granites) and granodiorite (comparable to parts of the gneissic granites). On the basis of kinematic data from shear zones in the marginal tonalite, and strain measurements using xenoliths, Ramsay concluded that

deformation occurred by ballooning emplacement of the different rock suites of the Chinamora batholith (with a small amount of diapirism). Different magma pulses of increasingly siliceous composition led to expansion of the previously crystallized granitoid rocks pushing aside the enveloping greenstone belt as well as earlier magma pulses.

The structure of the adjacent greenstone belt and parts of the Chinamora batholith was studied by Jelsma et al. (1993) who found many of the indicative criteria for diapirism. More recently, Dirks and Jelsma (1998) and Jelsma and Dirks (2000) recognized two different deformation and metamorphic events, D_1/M_1 and D_2/M_2. They proposed that D_2/M_2 diapir-related deformation and metamorphism follow an earlier, D_1/M_1 regional deformational and metamorphic event that affected the greenstone sequences.

According to Dirks and Jelsma (1998), the greenstone belt shows an early set of D_1/M_1 structures and fabrics and associated syn-kinematic greenschist to low amphibolite grade metamorphic assemblages. Structures include anastomosing networks of shear zones, characterized by S–C fabrics, rotated porphyroclasts, ribbon grains, rootless intrafolial or sheath folds, and very high strain intensities. The bedding-parallel schistosity or mylonitic fabric is defined by aligned mica, chlorite, amphibole, talc, serpentine or quartz-feldspar grains and is associated with a shallow, easterly or westerly plunging mineral or aggregate lineation defined by these same minerals. Jelsma and Dirks (2000) proposed that these were formed during an episode of layer-parallel shearing, imbricate stacking and recumbent folding of the greenstone stratigraphy. According to these authors, the D_1/M_1 event affected all greenstone belt formations including the youngest felsic volcanics dated at ca. 2643 Ma, but the event may have started already prior to this date.

D_2/M_2 fabrics, strain patterns and contact aureoles overprint those associated with D_1. The intensity of both the M_2 metamorphic overprint (in particular temperature) and the D_2 deformation fabric decrease away from the contact of the Chinamora and Murehwa batholiths into the adjacent greenstone belt (Jelsma, 1993), suggesting a causative relationship with the emplacement of the batholiths. Structural analyses in the contact area with the granitoid rocks revealed a marginal foliation parallel to the granite–greenstone contact, a radial lineation normal to the contact, high finite-strain intensities, triaxial flattening strains and kinematic data that have been explained by off-the-dome sliding of the greenstone strata (Jelsma et al., 1993). Porphyroclasts of andalusite and staurolite have grown syn-kinematically with respect to a phyllonitic foliation. Mineral ages on unoriented M_2 garnet (U–Pb) and hornblende (Ar–Ar) grains from the margin of the greenstone belt near the Murehwa batholith showed that the M_2 contact metamorphic overprint in this area related occurred between ca. 2.62 and 2.57 Ma (Van Dijk and Kater, 1996; Dirks and Jelsma, 1998; Siegesmund et al., in press).

3. Magnetic fabric in the Chinamora batholith

3.1. Methodology

The AMS of the granitic rocks of the Chinamora batholith was measured as a method frequently used for the structural mapping of granites (King, 1966; Hrouda, 1982; Hrouda and Lanza, 1989; Benn et al., 1997; Siegesmund and Becker, in press). Cylinders of 25 and 40 mm diameter were measured in an applied field of approximately 0.5 mT in 15 directions, thus a second rank tensor can be calculated that describes the magnetic anisotropies of the sample (see Jelinek 1977, 1981 for details). A geometric representation of the tensor is an ellipsoid with the three principal axes $k_x > k_y > k_z$. For the representation of measurement results the parameters P' (corrected degree of anisotropy), T and U (shape of the magnetic ellipsoid), L (degree of linear anisotropy) and F (degree of planar anisotropy) were used according to Jelinek (1981). The shape of the magnetic ellipsoid (T) can obtain values between -1 (corresponding to a perfect prolate magnetic ellipsoid) and 1 (corresponds to a perfect oblate magnetic ellipsoid) with a neutral field at $0.05 > T > -0.05$. Since the bulk susceptibility of some samples reached very high values, high field analyses (HFA) were applied to some selected samples to test the contribution of paramagnetic and ferrimagnetic minerals to the magnetic fabric. This was done by measuring the samples in fields above 800 mT with different field strengths using a torque magnetometer (Bergmüller et al., 1994; Bergmüller and Heller, 1995). The results of these measurements are presented in the factor U (shape of the magnetic ellipsoid) and can be compared to the measurements of the AMS data (the torque magnetometer only measures the deviatoric part of the tensor while in AMS measurements the tensor itself is measured).

The Curie-balance is a thermomagnetic measurement which is able to obtain qualitative values for the content of ore minerals. Therefore, a sample is measured in an applied field of approximately 550 mT at temperatures up to 700°C, which is above the Curie-temperature of most ore minerals. However, these measurements are not capable of determining the carrier of the magnetic fabric.

3.2. AMS measurements

3.2.1. Basement gneiss

The volume susceptibility of the basement gneisses is very low, compared to the other units. It ranges between 18×10^{-6} SI and 7000×10^{-6} SI, averaging 1095×10^{-6} SI (Fig. 6a). Most of the samples have moderate degrees of anisotropy (P' ~1.0–1.2, average ~1.12). They show a predominantly oblate shape of the magnetic ellipsoid, and fewer samples have neutral or prolate shapes (Fig. 6b). According to this the planar anisotropy is much better defined than the linear anisotropy. In Fig. 6c, the magnetic lineation generally has a subhorizontal plunge and weak

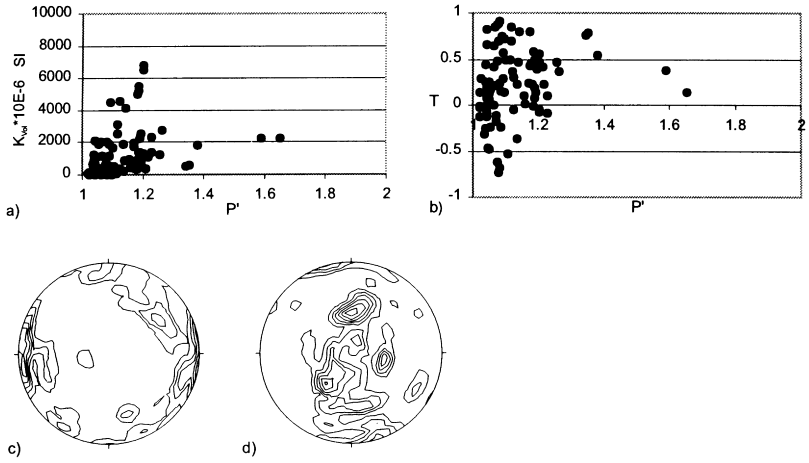

Fig. 6. Magnetic fabric of the possible basement gneisses. (a) The samples show a moderate degree of anisotropy. (b) Samples show a highly oblate shape of the magnetic ellipsoids indicating a well-developed magnetic foliation. (c) The magnetic lineation surmises an incomplete girdle in the pole figure. Sample density is low owing to the outcrop situation. (d) The flat-lying magnetic foliation has an E–W strike. Since the magnetic foliation is better defined, no sharp point-maxima can be observed.

point-maxima are developed in the pole figure. The magnetic foliation describes an incomplete girdle (Fig. 6d).

3.2.2. Gneissic granites

The southern gneissic granites show volume susceptibilities ranging between 500 and 7300×10^{-6} SI, averaging 1894×10^{-6} SI (Fig. 7a). Their degree of anisotropy ranges around 1.1 for the low susceptible samples, and higher volume susceptibilities can be roughly correlated with higher degrees of anisotropy. The shape of the magnetic ellipsoid of the samples ranges between moderately oblate and moderately prolate, and most of the samples yield values of $-0.5 < T < 0.5$ (Fig. 7b). Depending on the shape of the magnetic ellipsoids, the degree of planar anisotropy dominates the degree of linear anisotropy and vice versa. The northeastern gneisses have bulk susceptibilities of up to 5000×10^{-6} SI, averaging 2000×10^{-6} SI, and their degree of anisotropy averages 1.15 (Fig. 7c). Only a vague increase of the degree of anisotropy with increasing susceptibilities can be observed. The shape of the magnetic ellipsoid shows prolate to oblate shapes, but the majority of the samples plot in the oblate field (Fig. 7d). The northwestern gneissic granites show low volume susceptibilities, averaging 1375×10^{-6} SI (Fig. 7e). Their degree of anisotropy is low, compared to the other gneissic granites, averaging 1.09. The shape of the magnetic ellipsoids is moderate oblate to moderate prolate with a weak concentration of samples in the neutral to moderate oblate field (Fig. 7f).

The magnetic foliation in the gneissic granites tends to be parallel to the batholith margin, but is strongly oblique to internal lithological boundaries (Fig. 8). Only in the southern gneissic granites is the magnetic foliation not parallel to the margin of the batholith. The magnetic lineation in the gneissic granites has a very stable EW trend with most of the magnetic lineations plunging away from the center of the batholith (see Figs. 7g, i and 9). In the western gneisses the magnetic lineation plunges to the west, in the northeastern gneisses to the east, and in the southern gneisses to both directions (see Fig. 7g).

3.2.3. Equigranular granites

The equigranular granites in the western areas of the Chinamora batholith (near Mazowe dam) show volume susceptibilities in the range of $100–5000 \times 10^{-6}$ SI, averaging approximately 1550×10^{-6} SI. The samples can be divided into a group of low susceptible samples ($100–500 \times 10^{-6}$ SI) and high susceptible samples ($>1000 \times 10^{-6}$ SI, see Fig. 10a). The distribution of the volume susceptibilities seems to be irregular but the sample density is low owing to the inaccessibility of the area.

The degree of anisotropy ranges between 1.0 and 1.2, averaging 1.05. The shape (T) of the magnetic ellipsoids concentrates in the field of moderately oblate shapes ($T \sim 0.5$) indicating a dominating magnetic foliation; still some of the samples are strongly prolate with values as low as $T = -0.75$ (Fig. 10b). The degree of anisotropy is again not correlated with the shape of the magnetic ellipsoid (Fig. 10).

The pole figure of the magnetic lineation shows a broad maximum in the NW with moderately plunging angles (30–40°, Fig. 10c). The magnetic lineation is continuous across internal boundaries and it is oblique to the contact with the surrounding greenstone belt (Fig. 9). The magnetic foliation of the equigranular granites shows moderate to steep dips parallel to the outer margin of the batholith while internal lithological boundaries are cross-cut by the magnetic foliation (Fig. 8). The pole figure of the magnetic foliation shows two broad point-maxima (Fig. 10d). With a higher sample density in this area these point-maxima probably would be interconnected to form a girdle, as could be deduced from the margin-parallel strike.

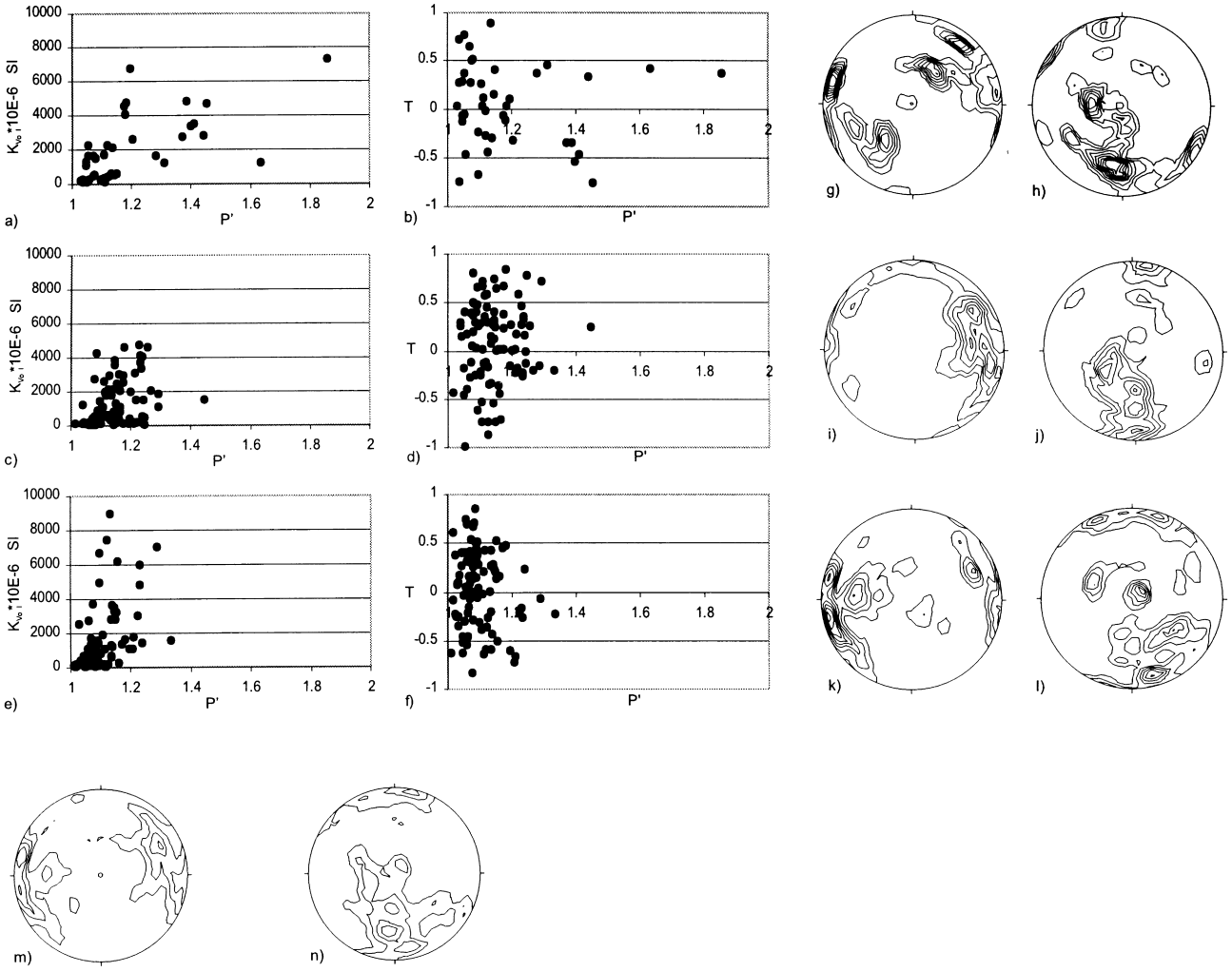

Fig. 7. Magnetic fabric of the gneissic granites. The results of the measurements have been divided into the southern gneisses (a–b, g–h), the northeastern gneisses (c–d, i–j) and the northwestern gneisses (e–f, k–l). In figures m and n the different gneisses have been analysed as a whole. Orientations of magnetic lineations (g, i, k) and foliations (h, j, l) are slightly rotated in the different gneisses; this probably is due to small changes in the tectonic environment during their emplacement. The southern gneissic granites have additionally been deformed during movement along the Umwindsi shear zone.

3.2.4. Porphyritic granite

The porphyritic granite in the central part of the batholith shows volume susceptibilities up to approximately 8000×10^{-6} SI. The calculated average volume susceptibility of the samples is 2767×10^{-6} SI; however, most of the samples show values ranging between 500×10^{-6} SI and 3000×10^{-6} SI (Fig. 11a). The degree of anisotropy (P') for most of the samples is very low (1.0–1.15), and only a few samples exceed a degree of anisotropy above 1.20. As in the gneissic granites, the samples with a high volume susceptibility do not necessarily show a high degree of anisotropy. The degree of anisotropy usually is only weakly related to the value of the volume susceptibility (Fig. 11a), and only samples with strong linear anisotropies can be correlated to high volume susceptibilities.

The shape of the magnetic ellipsoids (T) is very irregular and no preferred shape is obvious. The samples are uniformly distributed in both the prolate and oblate fields (Fig. 11b). The degree of anisotropy is not related to the shape of the magnetic ellipsoid. The calculated average linear anisotropy of the samples is moderate (1.07) and of the same magnitude as the planar anisotropy (1.06). Peaks of the linear anisotropy reach 1.24 and are then related to volume susceptibilities above 3000×10^{-6} SI, a very high degree of anisotropy (~1.4) and, of course, prolate shapes of the magnetic ellipsoid (Fig. 11b).

The magnetic lineation of the samples shows a very consistent ENE–WSW strike forming a good point-maximum in the pole figure. Angles of plunge are very low and hardly exceed values >30° (see Figs. 9 and 11c). Plotted as a pole figure (lower hemisphere) the magnetic foliation shows a broad N–S girdle with a maximum in the center of the pole figure (Fig. 11d). The dip of the magnetic foliation averages 20–40°, and lower or higher values are scarce. The magnetic foliation preferably dips to the SSW and usually does not follow the margins of the porphyritic

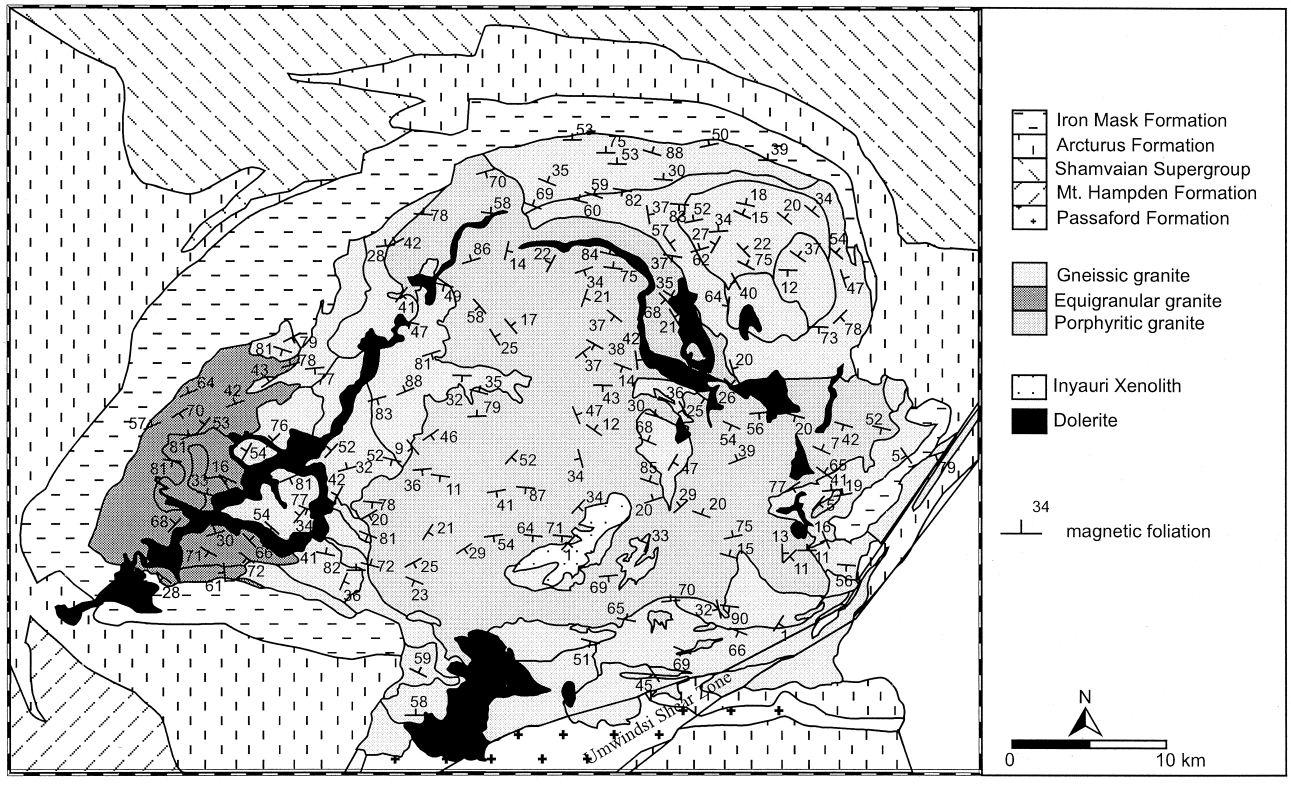

Fig. 8. Map of the magnetic foliation in the Chinamora batholith. Data were chosen for presentation according to their consistence from measurements of the same core (applies to Fig. 9 as well). Note the margin parallel strike of the foliation inside the gneissic granites and the stable EW trending foliation in the porphyritic granite. Solid lines indicate lithological boundaries.

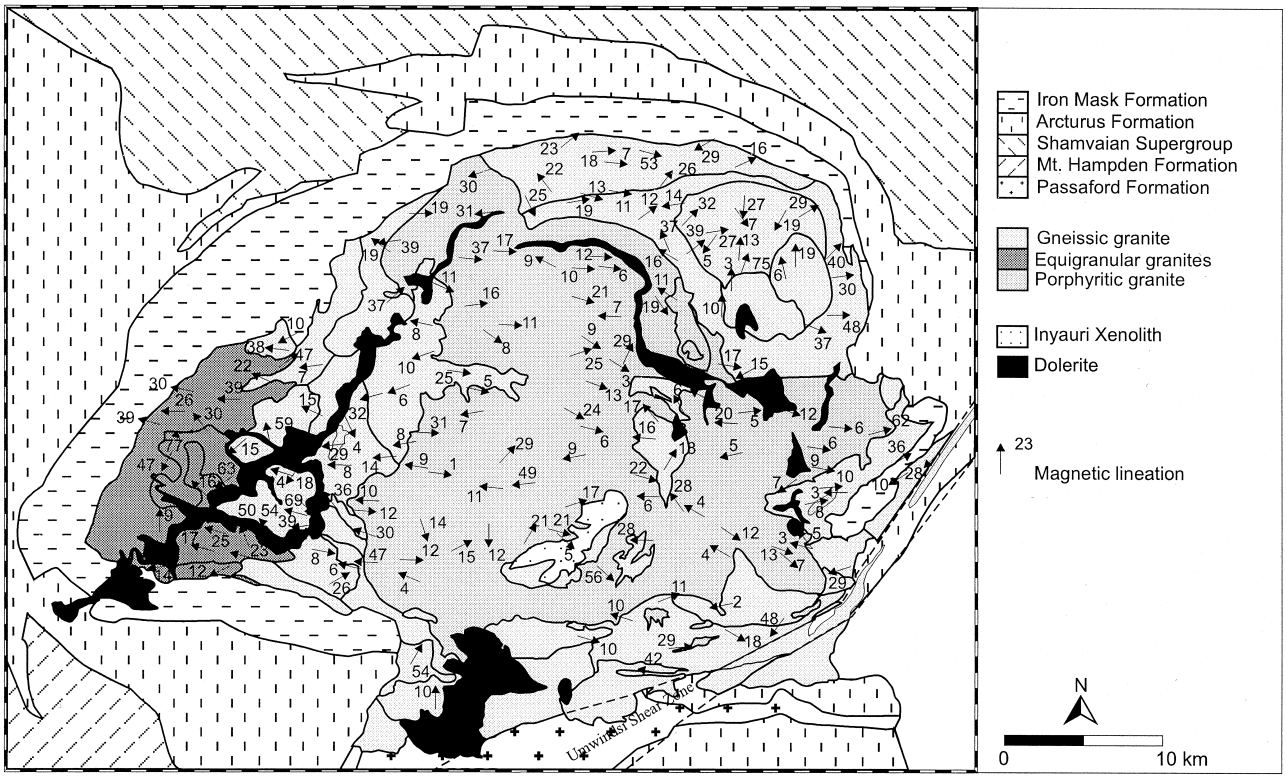

Fig. 9. Map of the magnetic lineations in the Chinamora batholith. Lineations trend EW throughout the batholith with low dipping angles. Note that dipping of lineation in the northeastern granites is mainly to the east while in the western granites magnetic lineation preferably dip to the west. The gneissic granites in the northeast show fabrics indicative of a small ballooning pluton intruded into the gneissic granites.

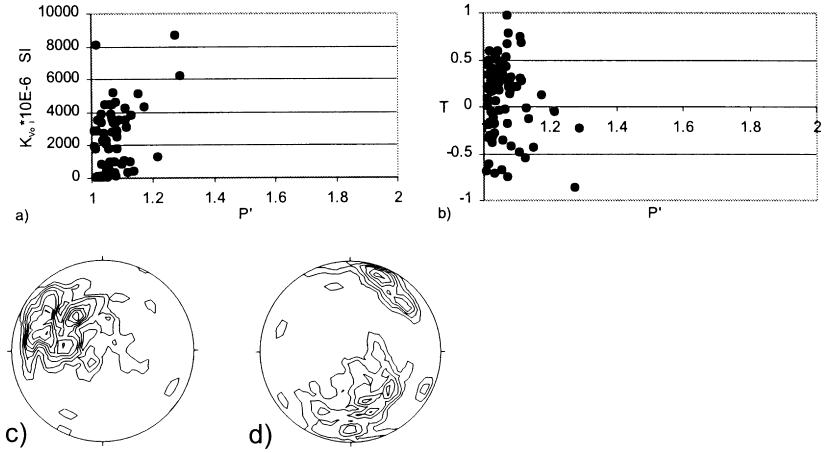

Fig. 10. AMS measurements for the equigranular granites. (a) Samples show moderate bulk susceptibilities and low degrees of anisotropy. (b) Most of the samples have moderate oblate shapes of their magnetic ellipsoids indicating a better defined magnetic foliation than magnetic lineation. (c) The magnetic lineation preferably dips to the NW with moderate dipping angles. (d) The magnetic foliation seems to build an incomplete girdle indicating a preferred margin parallel strike.

granite (see Fig. 8) but tends to form a funnel-shaped narrowing to the east.

3.3. Curie-balance

In total, 15 samples with various bulk susceptibilities have been selected for a qualitative measurement of their ore content. Samples with low bulk susceptibilities did not give good measurement results indicating, as expected, a neglectable content of ore minerals. Samples with high bulk susceptibilities all contain a ferrimagnetic phase indicated by the vanishing ferrimagnetic properties of the samples at temperatures of approximately 578°C, which is the Curie-temperature of magnetite. The presence of admixtures of hematite is indicated by the common horizontal deflection of the curve to temperatures around 625°C (Fig. 12). Since the most abundant ore mineral in the samples seems to be magnetite, a separation of the paramagnetic properties from the ferrimagnetic properties of the samples using HFA and AMS can be carried out.

3.4. Significance of magnetic rock fabric

To test the significance of the magnetic rock fabrics, two different approaches were used. Firstly, selected hand specimens were cut in three perpendicular directions according to the magnetic fabric. If the magnetic fabric corresponds to the macroscopic fabric the latter should be visible in the hand specimen. Secondly, HFA were carried out. HFA, together with the AMS data, may allow a separation of the ferrimagnetic and paramagnetic properties of the samples. If the measured values of the ferrimagnetic properties differ to

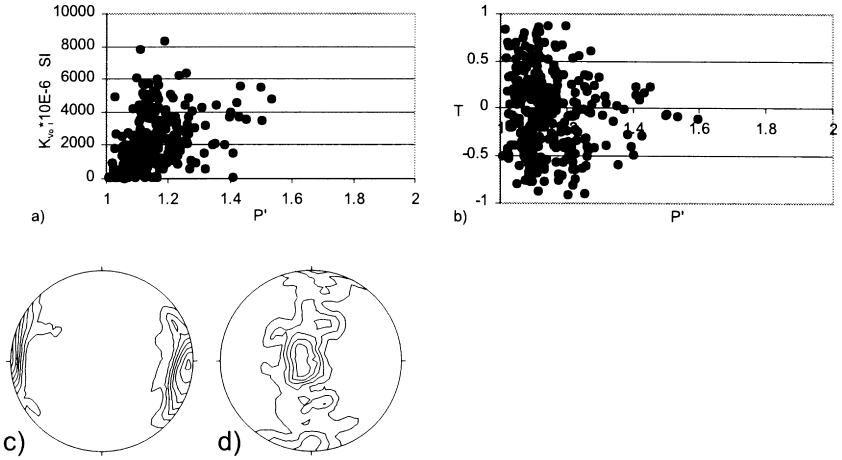

Fig. 11. Magnetic fabric of the porphyritic granite. (a) The bulk susceptibility as a function of the degree of anisotropy is widely scattered. Only a weak trend of increasing degrees of anisotropies with increasing bulk susceptibility is obvious. The shape of the magnetic ellipsoid (b) is also inconsistent. (c) The magnetic lineation in the porphyritic granites has a very narrow point maximum indicating flat-lying (subhorizontal) magnetic lineations with an E–W strike. (d) The magnetic foliation defines a girdle in the pole figure; however, the majority of the foliation planes are nearly horizontal.

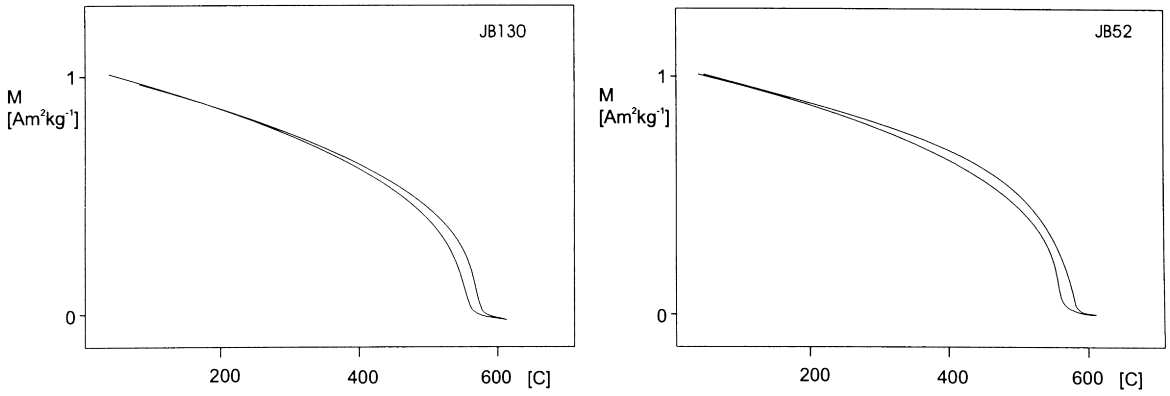

Fig. 12. Measurement curves of the Curie-balance from (a) sample JB130 and (b) sample JB52. See text for further details.

a greater extent from the paramagnetic properties, the sample is dominated by the ferrimagnetic properties. In this case, caution must be applied in the interpretation of the magnetic fabric of that sample if the ferrimagnetic properties do not mimic the paramagnetic properties (which is often the case if, for example, secondary magnetites develop through alteration of biotites).

The dominant characteristic of the gneissic granites in terms of macroscopic fabrics is a well-developed foliation defined by medium to small sized biotite flakes. The magnetic measurements do match the macroscopic foliation very well, and only the dip of the magnetic foliation seems to be steeper than the dip of the macroscopic foliation. Samples in the gneissic granites that only show a weak magnetic fabric (low *T*-values, low degrees of linear and planar anisotropy) show a weak macroscopic fabric as well. In the porphyritic granite the magnetic measurements revealed a wide variety of magnetic fabrics ranging from very well defined to nearly isotropic. The hand specimens of this unit usually show a pronounced alignment of feldspars with biotite flakes undulating around the feldspar grains. This explains the sometimes only weak coincidence of the magnetic and macroscopic fabric. It has been shown by Siegesmund et al. (1995) that biotites undulating around an axis perpendicular to the crystallographic *c*-axis produce neutral or even prolate shapes of the magnetic ellipsoids. Furthermore, the degree of magnetic lineation increases and the degree of magnetic foliation decreases through this undulation. The equigranular granites in the west of the batholith do not show a well-developed magnetic fabric, and for these samples no macroscopic fabric was visible in hand specimen.

The HFA measurements in some samples revealed a very good agreement between the orientation of the principal axes of the ferrimagnetic and paramagnetic components of the samples. They also were in agreement with the AMS measurements. Two examples are shown in Fig. 13: sample x1 (Fig. 13a) from the gneissic granites near the Umwindsi shear zone and sample JB99 (Fig. 13b) from the porphyritic granite. Sample x1 shows a good agreement between the AMS measurement and the ferrimagnetic properties of the sample while the paramagnetic axes of the magnetic ellipsoid are rotated with respect to the AMS measurement. The k_z-axes of all the different measurements are subparallel to each other, indicating that the ferrimagnetic fabric mimics the paramagnetic fabric, indicating both phases are flattened in the same plane. In sample JB99 the paramagnetic as well as the ferrimagnetic principal axes show an excellent agreement represented in the coaxial orientation of the respective magnetic axes. There is only a slight dominance of the ferrimagnetic properties over the paramagnetic properties, indicated by the parallel strike and plunge of the ferrimagnetic axes of the magnetic ellipsoid and the axes measured during AMS measurements. Still, the paramagnetic axes of

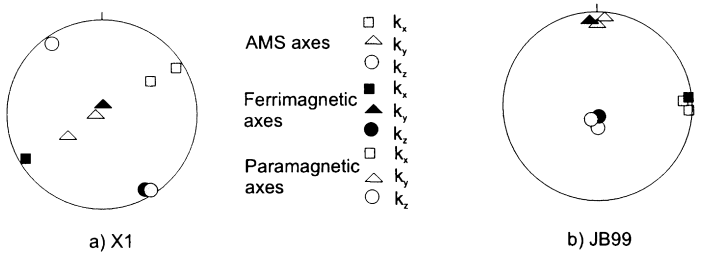

Fig. 13. (a) HF-analysis of sample x1. Ferrimagnetic axes of the magnetic ellipsoid and axes obtained from AMS measurements show a very good concordance while the paramagnetic axes are rotated with respect to the AMS measurements. (b) HF-analysis from sample JB99. The axes of the different properties and measurements all show a very good concordance.

the magnetic ellipsoid are subparallel to the ferrimagnetic axes.

4. Discussion and conclusions

The different intrusive units within the Chinamora batholith have been grouped into (i) basement gneisses; (ii) gneissic granites; (iii) equigranular granites; and (iv) porphyritic granites. The basement gneisses are banded in nature and are only exposed in isolated areas. A poorly constrained Rb–Sr age of 2865 ± 35 Ma suggests that these gneisses are older than any of the greenstone belt lithologies in the area and could represent either basement to the greenstones or a tectonically juxtaposed older crustal unit.

The gneissic granites (tonalites to syenogranites) occur near the outer margin of the Chinamora batholith. Their age of emplacement and crystallization must be younger than 2643 Ma (which is the age of extrusion of felsic volcanics in the adjacent greenstone belt), but older than 2601 Ma (which is the crystallization age of the porphyritic granites). The gneissic granites are characterized by a macroscopic biotite foliation that parallels the batholith margin, dipping outward at moderate angles, between 40 and 60°. The magnetic foliation also parallels the batholith margin, but is oblique to internal lithological boundaries. It has been folded around a magnetic lineation that has an E–W trend and that plunges at shallow angles away from the center of the batholith. The equigranular granites are not as well exposed as the gneissic granites but have a similar distribution, composition and magnetic fabric. Both the gneissic granites and equigranular granites show prolate and oblate shapes of the magnetic ellipsoid. We regard the equigranular granites as representing late intrusive phases but part of a longer continuous magmatic event that is dominated by the emplacement of the gneissic granites.

The porphyritic granites occur in the central part of the batholith and predominantly comprise monzogranites. They show distinctly different orientations of the macroscopic and magnetic fabrics as compared to the gneissic and equigranular granites. Magnetic fabrics are generally weak but include well-defined and isotropic varieties. The macroscopic and magnetic planar fabrics are defined by the alignment of biotite flakes and feldspar phenocrysts and trend NW–SE, dipping at moderate angles, predominantly to the SW. In places, their orientation is oblique to the margin of the porphyritic granite. The magnetic lineation is defined by biotite flakes undulating around the feldspar megacrysts and has an ENE–WSW trend. Following Wilson et al. (1995) and Jelsma et al. (1996), we regard these granites as a separate intrusive event. They resemble the Chilimanzi Suite granites in the eastern and southern parts of the craton in composition, field appearance and age (Frei et al., 1999).

Different tectono-magmatic models have been proposed for the emplacement of the Chinamora batholith and have been described above in the section on regional geology. Our data show that the gneissic and equigranular granites have distinctly different fabric orientations compared to the porphyritic granites. The macroscopic and magnetic foliations in the gneissic granites have a similar orientation and are continuous with the macroscopic foliation in the adjacent greenstone wall rocks, indicating that they are cogenetic. Emplacement of the porphyritic granites postdates the formation of this foliation. This foliation corresponds to the S_2 foliation of Jelsma and Dirks (2000) within the greenstone wall rocks. It is penetrative at the actual batholith–greenstone contact and is associated with a radial mineral lineation (L_2), high finite strain intensities and shear sense indicators that show a consistent normal, dome-side-up sense of movement (Jelsma et al., 1993). M_2 contact metamorphic aureoles are concentric around the batholith and pass continuously into regional M_1 metamorphic isograds. Together, these structural and metamorphic features cannot be explained by models invoking non-cylindrical folding or core complexes, and suggest either intrusion of granitoids into a growing antiform, causing a contact metamorphic overprint, or (syn-tectonic?) diapiric or ballooning emplacement of the granitoids, having a similar effect.

Ramsay's (1989) strain data for the gneissic granites, equigranular granites and porphyritic granites indicated a flattening type of strain, which may be typical for an inflating, ballooning pluton (Clemens et al., 1997). However, his strain measurements were done on horizontal surfaces, largely assuming that $X{:}Z = Y{:}Z$. He calculated high strain values in the gneissic granites in the southern and eastern parts of the batholith and generally low strain values for the rest of the batholith. The highest strain values that he recorded occurred near the Umwindsi shear zone, represent solid-state deformation, and should potentially be taken separately from the database that is used to model the emplacement of the batholith. He also found that the gneissic and equigranular granites are characterized by conjugate sets of relatively small-scale shear zones. The kinematics of these shear zones can be explained with a margin parallel direction of maximum expansion. These shear zones may have developed through the expansion of the batholith by an injection of the porphyritic granite into the consolidated gneissic granites (Ramsay, 1989), but they could also have developed as a result of the diapiric or ballooning emplacement of the gneissic granites (Jelsma et al., 1993).

An investigation of the strain in the contact zone of the Chinamora batholith and the greenstone belt was done by Jelsma et al. (1993) using a variety of strain markers. They calculated high strain intensities and triaxially flattening types of strain requiring components of pure and simple shear. The upward movement of the batholith with respect to the greenstone succession cannot be explained by a model that envisages solely ballooning since a ballooning pluton or batholith is inflated at the point of intrusion (Clemens et al.,

1997). From a strictly geometric point of view a balloon has a roughly spherical shape. If we assume a balloon diameter of about 30 km (which is close to the current diameter of the batholith), the batholith may have extended close to the upper mantle (since the Zimbabwe craton is only 30–35 km thick; Blenkinsop et al., 1997), which is highly unlikely.

From the observed magnetic fabric and the structural relationships we envisage the different gneissic granites and the equigranular granites to represent distinct plutons (batch melting of the same source?) that together make up a composite batholith that was emplaced syntectonically as a (blistering or domal?) diapir, perhaps with some ballooning component.

The origin of the E–W linear fabric in the gneissic granites remains to a certain degree enigmatic. The scatter of degree of anisotropy and the shapes of the respective magnetic ellipsoids cannot solely be explained by different contributions of the respective mineral fabric (e.g. alignment of hornblendes or parallel orientations of biotites) and must be explained by the effects of an external stress field. Furthermore, from microscopic analyses and the measurements of the Curie-balance it appears that high degrees of anisotropy and the corresponding shapes of the magnetic ellipsoids are influenced by the interaction of magnetite grains as well. This applies to all the observed units in the batholith.

This magnetic lineation is not collinear with the radial, L_2 macroscopic lineation in the wall rocks. It has a general E–W trend with shallow angles of plunge away from the center of the batholith. Similarly oriented lineations can be found in the greenstone belts throughout the northern parts of the Zimbabwe craton (Shamva, Dindi, Makaha; Jelsma and Dirks, 2000), indicating that emplacement of the gneissic granitoids may have taken place syn-tectonically during a far-field compressional event. In these belts, the E–W lineation is early and associated with layer-parallel shear zones that accommodated east over west stacking and duplication of the crust. According to Jelsma and Dirks (2000), this lineation represents the transport direction during the D_1 deformational event.

Emplacement of the central porphyritic granites cannot be accomplished through diapirism. Evidence for a sheet-like structure of the porphyritic granite comes from erosional windows in which gneisses outcrop in the porphyritic granite, small occurrences of porphyritic granite in the area of the gneissic granites in the south, and the fact that the porphyritic granite can only be found above a certain elevation. Based on this, the porphyritic granite is either eroded down to the floor region of the intrusion or it has been a sheet-like intrusion from the beginning. Diapiric or ballooning emplacement can be excluded on the basis of the lack of vertical lineations that mark the ascent path of the magma and the absence of a margin parallel fabric. However, foliations in the porphyritic granite are not horizontal as would be expected for a sheet-like intrusion or for the floor region of a larger magmatic body.

Snowden and Bickle (1976) used the deflection of megacryst alignments around the Inyauri xenolith to conclude that the porphyritic granites were deformed during two regional folding events. However, we have shown that emplacement of the porphyritic granites postdates the D_2 deformational event in the greenstone wall rocks, which is the last major deformational event for these rocks. Jelsma et al. (1993) suggested that the deflection of the feldspar megacryst alignment can better be ascribed to magmatic flow rather than to cross-folding.

Recently, Blenkinsop et al. (1999) described small-scale folding of pegmatite layers, mafic schlieren and local contacts between subphases in the porphyritic granite. They explained these folds to be the product of syn-magmatic deformation. The folds have wavelengths of several meters and have axes that plunge generally ENE. This orientation of the fold axes is collinear with the magnetic lineations that we measured for the porphyritic granites. However, our magnetic foliations show that the overall geometry of the porphyritic granites is that of an inclined sheet, ruling out the existence of large-scale folds. We acknowledge that localized small-scale folding of the porphyritic granites has occurred, but ascribe this to emplacement of the porphyritic granites during the waning stages of the D_2 event.

The porphyritic granite shows moderately inclined foliation planes preferably dipping to the southeast. Only in the extreme southeast is a steeply inclined foliation dipping north visible. The E–W lineation in this unit shows the same stable trend as in the gneissic granites. The erosional windows and the Inyauri xenolith in the underlying gneisses seem to point to a thin sheet rather than a thick body. These fabrics and field observations are best explained through emplacement of the magma as a laccolith that may have been fed by dyke-like conduits as proposed by Treloar (1997). In their experiments on simplified models of magma emplacement Roman-Berdiel et al. (1995) found a linear correlation between the thickness of the brittle overburden, the diameter of the intrusion and the thickness of the emplaced laccolith. According to these experiments the porphyritic granite with its overburden (surrounding greenstones) of approximately 10 km leads to a laccolith diameter of 28 km which matches today's outcrop area of the porphyritic granite. From the correlation of thickness of overburden and thickness of laccolith a thickness of 3 km is estimated for the porphyritic granite. The proposed shape of the porphyritic granite during emplacement is that of a NE verging laccolith.

In summary, the proposed emplacement history of the Chinamora batholith firstly includes the ascent of the now gneissic granites and equigranular gneisses, during a far-field compressional event (see Fig. 14). Cumulative emplacement of the different subphases of these two units was through a large-scale (blistering or domal?) diapir with a diameter that is very similar to the present-day diameter of the Chinamora batholith. Some of the deformation of the

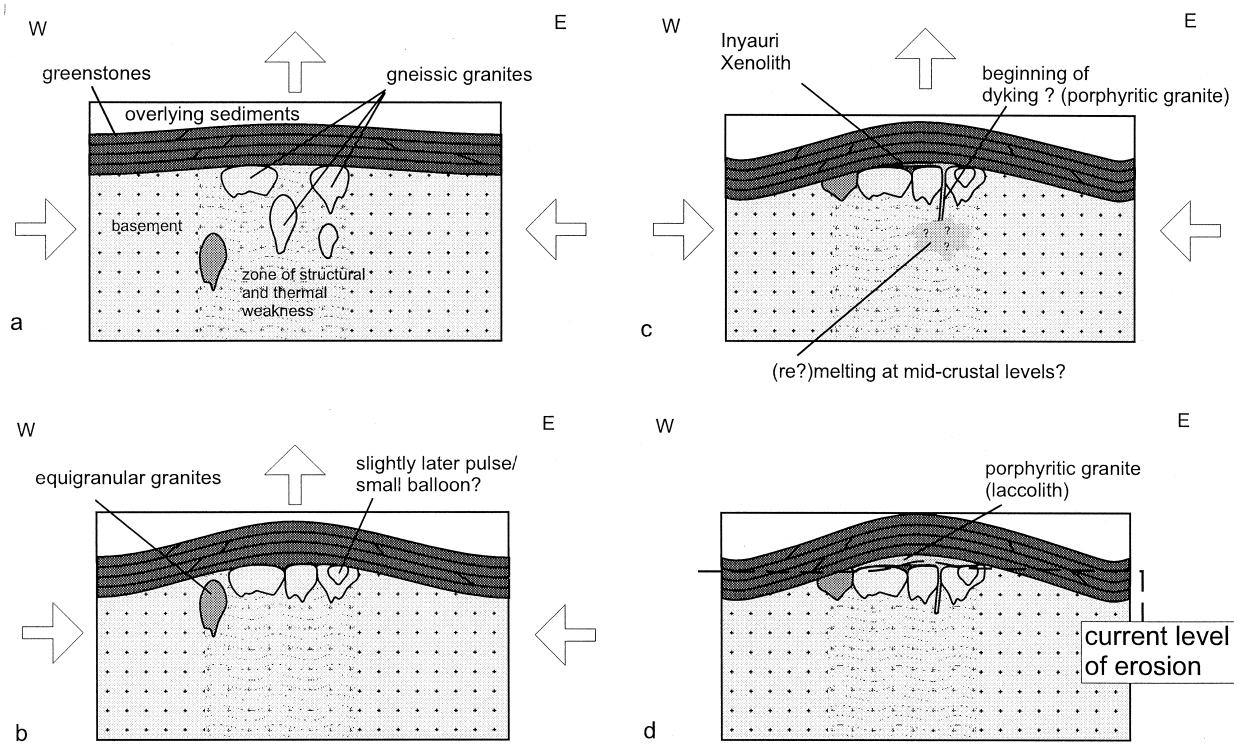

Fig. 14. Possible ascent and emplacement history of the granitoid rocks in the Chinamora batholith. Rising of the now gneissic granites as small diapirs led to the formation of the varying lithologies and caused structural weakness of the crust probably accompanied by elevated temperatures. This may have enhanced melting of a yet unknown source and led to the dyking (?) of the porphyritic granite which is emplaced as a laccolith on top of the gneissic and equigranular granites. The greenstone belts have been deformed prior to and during the intrusion of granitoids.

adjacent wall rocks can be attributed to ballooning expansion. The ascent and emplacement was of importance for the formation of the dome-and-keel configuration of the granite–greenstone terrain. This event must have happened after 2.64 Ga but before 2.60 Ga. After emplacement, the southern gneissic granites have been strongly deformed in the solid state as a result of oblique movements along the Umwindsi shear zone. The last major magmatic event at ca. 2.6 Ga is the emplacement of the (Chilimanzi type) porphyritic granites as a laccolith (Fig. 14). The fact that the gneisses as well as the porphyritic granite are comparable to other granitoids in the Zimbabwe craton (Wedza Suite and Chilimanzi Suite, Jelsma 1993) indicates that the generation, ascent and emplacement of the granites are a direct consequence of complex tectono-magmatic processes that affected the craton as a whole.

Acknowledgements

J.K. Becker would like to thank F. Heller for the measurement time in the excellent magnetic lab at the ETH Zurich and F.M. Hernandez for her corrections of the measurement routines of the HFA. S. Siegesmund thanks the German Science Foundation (DFG) for the grant SI-438/11 and for a Heisenberg fellowship. H.A. Jelsma is financially supported by grants from the Stiching Schurmannfonds (1997-199/13) and the University of Zimbabwe Research Board (RB/88/97). K. Benn and A.M. Hirt are thanked for the constructive reviews.

References

Baldock, J.W., 1990. The geology of the Harare greenstone belt and surrounding granitic terrain. Bulletins of the Zimbabwe Geological Survey 94.

Baldock, J.W., Evans, J.A., 1988. Constraints on the age of the Bulawayan Group metavolcanic sequences Harare greenstone belt, Zimbabwe. Journal of African Earth Science 7, 795–804.

Bateman, R., 1984. On the role of diapirism in the segregation, ascent and final emplacement of granitoid magmas. Tectonophysics 110, 211–231.

Benn, K., Horne, R.J., Kontak, D.J., Pignotta, G.S., Evans, N.G., 1997. Syn-acadian emplacement model for the South Mountain batholith, Meguma Terrane, Nova Scotia: magnetic fabric and structural analyses. Geological Society of America Bulletin 19, 1279–1293.

Bergmüller, F., Heller, F., 1995. The field dependence of magnetic anisotropy parameters derived from high-field torque measurements. Physics of Earth and Planetary Interiors 96, 61–76.

Bergmüller, F., Bärlocher, C., Grieder, M., Heller, F., Zweifel, P., 1994. A torque magnetometer for measurement of the high field anisotropy of rocks and crystals. Measurement Science and Technology 5, 1466–1470.

Bickle, M.J., Bettenay, L.F., Boulter, C.A., Groves, D.I., Morant, P., 1980. Horizontal tectonic interaction of an archean gneiss belt and greenstones, Pilbara Block, Western Australia. Geology 8, 525–529.

Blenkinsop, T., Martin, A., Jelsma, H.A., Vinyu, M.L., 1997. The Zimbabwe Craton, Southern Africa. In: deWit, M.J., Ashwal, L.D.

(Eds.), Greenstone Belts. Oxford University Press, Oxford, pp. 562–574.

Blenkinsop, T.G., Treloar, P.J. and Hanson, R., 1999. Rheology of granite magmas during emplacement: synmagmatic folding and magmatic axial planar fabrics in the Chilimanzi granites of the Zimbabwe craton. Abstract, meeting on deformation mechanisms and microstructures, Neustadt-am-Rhein, March, 1999.

Bouhallier, H., Choukroune, P., Ballevre, M., 1993. Diapirism, bulk homogeneous shortening and transcurrent shearing in the Archean Dharwar Craton: the Holenarsipur area, southern India. Precambrian Research 63, 43–58.

Bouhallier, H., Chardon, D., Choukroune, P., 1995. Strain patterns in Archean dome-and-basin structures: the Dharwar Craton (Karnataka, South India). Earth and Planetary Science Letters 135, 57–75.

Brun, J.P., Pons, J., 1981. Strain patterns of pluton emplacement in a crust undergoing non-coaxial deformation, Sierra Morena, Southern Spain. Journal of Structural Geology 3, 219–229.

Clemens, J.D., Mawer, C.K., 1992. Granitic magma transport by fracture propagation. Tectonophysics 204, 339–360.

Clemens, J.D., Petford, N., Mawer, C.K., 1997. Ascent mechanisms of granitic magmas: causes and consequences. In: Holness, M.B. (Ed.), Deformation-enhanced Fluid Transport in the Earth's Crust and Mantle. Chapman and Hall, London.

Collins, W.J., 1989. Polydiapirism of the Archaean Mount Edgar Batholith, Pilbara Block, Western Australia. Precambrian Research 43, 41–62.

Collins, W.J., Van Kranendonk, M.J., Teyssier, C., 1998. Partial convective overturn of archean crust in the east Pilbara Craton, Western Australia: driving mechanisms and tectonic implications. Journal of Structural Geology 20, 1405–1424.

Cruden, A.R., 1988. Deformation around a rising diapir modeled by creeping flow past a sphere. Tectonics 7, 1091–1110.

Dirks, P.H.G.M., Jelsma, H.A., 1998. Horizontal accretion leading to stabilization of the archean Zimbabwe Craton. Geology 26, 11–14.

Dixon, J.M., 1975. Finite strain and progressive deformation in models of diapiric structures. Tectonophysics 28, 89–124.

Dixon, J.M., Summers, J.M., 1983. Patterns of total and incremental strain in subsiding troughs; experimental centrifuged models of inter-diapir synclines. Canadian Journal of Earth Sciences (Journal Canadien des Sciences de la Terre) 20, 1843–1861.

England, R.W., 1990. The identification of granitic diapirs. Journal of the Geological Society of London 147, 931–933.

Eskola, P.E., 1947. The problem of mantled gneiss domes. Quarternary Journal of the Geological Society of London 104, 461–476.

Frei, R., Blenkinsop, T.G., Schönberg, R., 1999. Geochronology of the late Archean Razi and Chilimanzi suites of granites in Zimbabwe: implications for the late Archaean tectonics of the Limpopo belt and Zimbabwe craton. South African Journal of Geology 102, 55–63.

Hickman, A.H., 1984. Archean diapirism in the Pilbara Block, Western Australia. In: Kröner, A., Greiling, R.E. (Eds.), Precambrian Tectonics Illustrated. Schweizerbart'sche Verlagsbuchhandlung (Nägele u. Obermiller), Stuttgart, pp. 113–127.

Hogan, J.P., Gilbert, M.C., 1995. The A-type Mount Scott Granite sheet: importance of crustal magma traps. Journal of Geophysical Research 100, 15779–15792.

Hogan, J.P., Price, J.D., Gilbert, M.C., 1998. Magma traps and driving pressure—consequences for pluton shape and emplacement in an extensional regime. Journal of Structural Geology 20, 1155–1168.

Hrouda, F., 1982. Magnetic anisotropy of rocks and its application in geology and geophysics. Geophysical Survey 5, 37–82.

Hrouda, F., Lanza, R., 1989. Magnetic fabric in the Biella and Traversella stocks (periadriatic line): implications for the emplacement mode. Physics of the Earth and Planetary Interiors 56, 337–348.

Huizenga, J.M., 1995. Fluid evolution in shear zones from the late Archean Harare-Shamva-Bindura greenstone belt (NE Zimbabwe). Ph.D. thesis, Free University of Amsterdam.

Jelinek, V., 1977. The statistical theory of measuring anisotropy of magnetic susceptibility of rocks and its application. Geofyzika Brno, Czech Republic.

Jelinek, V., 1981. Characterization of the magnetic fabrics in rocks. Tectonophysics 79, 63–67.

Jelsma, H.A., 1993. Granites and greenstones in northern Zimbabwe: tectono-thermal evolution and source regions. Ph.D. thesis, Free University of Amsterdam.

Jelsma, H.A., Dirks, P.H.G.M., 2000. Structural geometries of a greenstone sequence in Zimbabwe: a product of crustal amalgamation and diapirism. Tectonics 19, 135–152.

Jelsma, H.A., Van Der Beek, P.A., Vinyu, M.L., 1993. Tectonic evolution of the Bindura-Shamva greenstone belt (Zimbabwe): progressive deformation around ballooning diapirs. Journal of Structural Geology 15, 163–176.

Jelsma, H.A., Vinyu, M.L., Valbracht, P.J., Davies, G.R., Wijbrans, J.R., Verdurmen, E.A.T., 1996. Constraints on Archean crustal evolution of the Zimbabwe Craton: a U–Pb zircon, Sm–Nd and Pb–Pb whole rock isotope study. Contributions to Mineralogy and Petrology 124, 55–70.

King, R.F., 1966. The magnetic fabric of some Irish granites. Geological Journal 5, 43–66.

Lister, G.S., Davis, G.A., 1989. The origin of metamorphic core complexes and detachment faults formed during Tertiary continental extension in the northern Colorado River region, U.S.A. Journal of Structural Geology 11, 65–94.

Macgregor, A.M., 1951. Some milestones in the Precambrian of Southern Rhodesia. Proceedings of the Geological Society of South Africa 54, 27–71.

Mareschal, J.C., West, G.F., 1980. A model for Archean tectonism; Part 2, Numerical models of vertical tectonism in greenstone belts. Canadian Journal of Earth Sciences (Journal Canadien des Sciences de la Terre) 17, 60–71.

Myers, J.S., Watkins, K.P., 1985. Origin of granite-greenstone patterns, Yilgarn Block, Western Australia. Geological Society of America (GSA) Geology (Boulder) 13, 778–780.

Paterson, S.R., Tobisch, O.T., 1988. Analysis and interpretation of composite foliations in areas of progressive deformation. Journal of Structural Geology 10, 745–754.

Platt, J.P., 1980. Archean greenstone belts: a structural test of tectonic hypotheses. Tectonophysics 65, 127–150.

Ramsay, J.G., 1989. Emplacement kinematics of a granite diapir: the Chindamora batholith, Zimbabwe. Journal of Structural Geology 11, 191–209.

Ridley, J., Vearncombe, J.R., Jelsma, H.A., 1997. Relations between greenstone belts and associated granitoids. In: deWit, M.J., Ashwal, L.D. (Eds.), Greenstone Belts. Oxford University Press, Oxford, pp. 376–397.

Roman-Berdiel, T., Gapais, D., Brun, J.P., 1995. Analogue models of laccolith formation. Journal of Structural Geology 17, 1337–1346.

Schmeling, H., Cruden, A.R., Marquart, G., 1988. Finite deformation in and around a fluid sphere moving through a viscous medium; implications for diapiric ascent. Tectonophysics 149, 17–34.

Schwerdtner, W.M., 1990. Structural tests of diapir hypotheses in Archean crust of Ontario. Canadian Journal of Earth Sciences (Journal Canadien des Sciences de la Terre) 27, 387–402.

Schwerdtner, W.M., Troeng, B., 1978. Strain distribution within arcuate diapiric ridges of silicone putty. Tectonophysics 50, 13–28.

Siegesmund, S., Becker, J.K., in press. The emplacement of the Ardara pluton (Ireland): new constraints from magnetic fabrics, rock fabrics and age dating. International Journal of Earth Science.

Siegesmund, S., Ullemeyer, K., Dahms, M., 1995. Control of magnetic rock fabrics by mica preferred orientation: a quantitative approach. Journal of Structural Geology 17, 1601–1613.

Siegesmund, S., Jelsma, H., Becker, J., Davies, G., Layer, P., van Dijk, E., Kater, L., Vinyu, M., in press. Constraints on the timing of granite emplacement, oleformation and metamorphism in the Shamva area, Zimbabwe. International Journal of Earth Science.

Snowden, P.A., 1976. The geology of the granitic terrain north and east of

Salisbury, with particular reference to the Chinamora batholith. Ph.D. thesis, University of Zimbabwe, Harare.

Snowden, P.A., Bickle, M.J., 1976. The Chinamora batholith: diapiric intrusion or interference fold? Journal of the Geological Society of London 132, 131–137.

Snowden, P.A., Snowden, D.V., 1979. Geology of an archean batholith, the Chinamora batholith-Rhodesia. Transactions of the Geological Society of South Africa 82, 7–22.

Snowden, P.A., Snowden, D.V., 1981. Petrochemistry of the late archean granites of the Chinamora batholith, Zimbabwe. Precambrian Research 16, 103–129.

Treloar, P.J., 1997. The generation, ascent and emplacement of granitic magmas: a Zimbabwean perspective. Abstract volume of the conference "Intraplate magmatism and tectonics of southern Africa", p. 51, Harare, Zimbabwe.

Van Berkel, J.T., 1988. Kinematic evaluation of a finite-element model of a diapiric ridge. Bulletin of the Geological Institute of the University of Uppsala 14, 111–114.

Van den Eeckhout, B., Grocott, J., Vissers, R., Bateman, R., 1986. On the role of diapirism in the segregation, ascent and final emplacement of granitoid magmas; discussion and reply. Tectonophysics 127, 161–169.

Van Dijk, E., Kater, L., 1996. Geology and metamorphic evolution of the Shamva greenstone belt, northeastern Zimbabwe. Internal report, Free University of Amsterdam.

Veenhof, R.P., Stel, H., 1991. A cleavage triple point and its mesoscopic structures; the Mustio Sink (Svecofennides of SW Finland). Precambrian Research 50, 269–282.

Vigneresse, J.L., 1995. Control of granite emplacement by regional deformation. Tectonophysics 249, 173–186.

Weinberg, R.F., Schmeling, H., 1992. Polydiapirs: multiwavelength gravity structures. Journal of Structural Geology 14, 425–436.

Weinberg, R.F., Podladchikov, Y., 1994. Diapiric ascent of magmas through power law crust and mantle. Journal of Geophysical Research, B. Solid Earth and Planets 99, 9543–9559.

Wilson, J.F., Nesbitt, R.W., Fanning, C.M., 1995. Zircon geochronology of Archean felsic sequences in the Zimbabwe craton: a revision of greenstone stratigraphy and a model for crustal growth. Geological Society Special Publication 95, 109–126.

Zeegers, T.E., White, S.H., de Keijzer, M., Dirks, P., 1996. Extensional structures during deposition of the 3460 Ma Warrawoona Group in the eastern Pilbara Craton, Western Australia. Precambrian Research 80, 89–105.